Journal of Structural Geology 32 (2010) 1187–1200

Contents lists available at ScienceDirect

Journal of Structural Geology

journal homepage: www.elsevier.com/locate/jsg

# Forward modeling synsedimentary deformation associated with a prograding steep-sloped carbonate margin

Phillip G. Resor [a,*], Eric A. Flodin [b]

[a] Department of Earth and Environmental Sciences, Wesleyan University, 265 Church Street, Middletown, CT 06459, USA
[b] Chevron Energy Technology Company, 6001 Bollinger Canyon Road, San Ramon, CA 94583, USA

ARTICLE INFO

*Article history:*
Received 1 February 2008
Received in revised form
9 April 2009
Accepted 27 April 2009
Available online 8 May 2009

*Keywords:*
Carbonate deformation
Synsedimentary deformation
Geomechanics
Permian Capitan reef
Guadalupe Mountains

ABSTRACT

Differential compaction associated with prograding and aggrading steep-sloped carbonate margins leads to penecontemporaneous and post-depositional modifications of stratal geometries and tensile and shear stress concentrations that might result in brittle deformation. In an effort to investigate controls on these deformation processes, we employ a step-wise gravity loaded elastic model that captures pre-failure displacement and stress field patterns for a depositional geometry based on the Permian Capitan depositional system, Guadalupe Mountains, West Texas and New Mexico, USA. We consider four model geometries with varying progradation to aggradation (P/A) ratios, from strongly prograding (P/A = 10) to strongly aggrading (P/A = 0.1). The strongly prograding case (P/A = 10) is used for sensitivity analysis that investigates the effects of varying rock mechanical properties of basin and platform facies. Model results yield relatively consistent patterns of deformation and stress that include: (1) a region of enhanced subsidence centered near the platform margin, (2) basinward displacement of the platform margin that decreases down slope, and (3) positive maximum Coulomb stress and positive (tensile) stress, both in-plane and out-of-plane, near the platform margin and in adjacent slope and platform facies. The patterns of deformation for the strongly progradational model are strikingly similar to present day stratal geometries of the Capitan depositional system that are often inferred to be primarily depositional in origin. Model results suggest that these geometries are established immediately upon deposition and may therefore affect the stratal architecture of the margin, but significant additional deformation also occurs during subsequent platform growth. We interpret the regions of positive Coulomb stress and tensile stress as areas likely to fail by faulting or jointing, respectively. This inference is corroborated by field observations of early-formed brittle deformation features in the Capitan margin. Our geomechanical models of the Capitan margin suggest that early-formed deformation is an integral part of the general steep-sloped carbonate system.



## 1. Introduction

Prograding carbonate platforms often aggrade hundreds of meters above their associated basin floors and develop high-relief margins with moderate to steep slopes. Carbonate platforms thus exert significant vertical loads on underlying fine-grained slope and basin sediments and also have the potential to extend horizontally in association with the slope face. These processes may cause significant synsedimentary deformation that can create additional accommodation space, modify depositional geometries, and generate faults and joints. Predictive models of these processes have the potential to improve understanding of early fracture formation that may be important in hydrocarbon migration and storage and interpretation of reef ecology and stratal architecture.

Compaction-induced differential subsidence likely plays a significant role in the development of carbonate platform geometries and sequence stratigraphy (Hunt et al., 1996; Playford, 1984). Experimental studies have demonstrated that carbonate sediments may undergo significant compaction during burial. Mud-rich shallow water carbonates may lose more than 50% of their volume during the first ~200 m of burial (Goldhammer, 1997; Shinn et al., 1977; Shinn and Robbin, 1983). Carbonate sands, while compacting less at shallow depths due to limited potential for grain reorientation and dewatering, may experience significant volume loss due to grain breaking and pressure solution at burial depths greater than a few hundred meters (Fruth et al., 1966; Goldhammer, 1997). Down-hole investigations (Audet, 1995; Budd, 2001, 2002;

* Corresponding author. Tel.: +1 860 685 3139; fax: +1 860 685 3651.
*E-mail addresses:* presor@wesleyan.edu (P.G. Resor), eflodin@chevron.com (E.A. Flodin).

0191-8141/$ – see front matter © 2009 Elsevier Ltd. All rights reserved.
doi:10.1016/j.jsg.2009.04.015

Halley and Schmoker, 1983; Heydari, 2000) have corroborated these experimental results, demonstrating significant porosity and permeability loss associated with mechanical and chemical compaction during the burial of carbonate sediments. Boundstones and early cemented sediments such as hard grounds, however, may retain much of their original volume, due to the presence of a relatively rigid framework. Lateral variations in carbonate facies and cementation may thus lead to significant variations in compaction across a carbonate shelf and slope.

The effects of differential compaction of carbonate sediments may include tilting of beds, the development of internal unconformities and sediment onlap (Hunt et al., 1996; Rusciadelli and Di Simone, 2007), and synsedimentary jointing (Devaney et al., 1986; Frost and Kerans, 2009; Guidry et al., 2007; Playford, 1984; Stanton and Pray, 2004) and faulting (Hunt et al., 2002; Kosa and Hunt, 2005). These effects are most clearly demonstrable in examples where uniform originally flat-lying strata overlie lateral variations in carbonate facies and are warped down over more compactable units (e.g. Anderson and Franseen, 1991). Differential compaction has also been suggested as a mechanism for generating basinward dips of platform strata associated with a number of carbonate platforms (Hunt and Fitchen, 1999; Longley, 1999; Rusciadelli and Di Simone, 2007; Saller, 1996). Alternatively, it has been suggested that basinward dipping strata may represent the original depositional geometry (e.g. Hurley, 1989; Kerans and Tinker, 1999; Osleger, 1998).

Efforts to model the effects of differential compaction have been largely conceptual or have treated compaction as a one-dimensional process driven purely by overburden mass (e.g. Longley, 1999; Saller, 1996). In situations of rapid sedimentation lateral fluid flow may become important (Dugan and Flemings, 2000) and reasonable consideration of compaction requires coupling between compaction and fluid flow (Bitzer, 1999). Furthermore, early cementation of carbonate strata (Grammer et al., 1993) may lead to lateral transmission of compaction-related stresses and strains within the cemented sedimentary layers. Modeling compaction of rapidly prograding carbonate platforms is thus likely to require at least two-dimensional mechanical considerations.

Extension or collapse associated with carbonate platform margins may also be a significant cause of synsedimentary deformation (e.g. Bosellini, 1998; George et al., 1995; Hine et al., 1992) and may create joints and sediment-filled dikes in recently deposited sediments (Playford, 1984). Carbonate slopes are typically steeper than siliciclastic slopes and have concave-up profiles (Kenter, 1990; Schlager and Camber, 1986). Rapid cementation may lead to slopes that exceed the angle of repose for loose sediment (Grammer et al., 1993). Steep carbonate slopes are thus metastable; supported by cohesion rather than frictional contact. Self erosion may further steepen slopes and generate the concave-up profile (Schlager and Camber, 1986). A variety of mechanisms have been suggested for triggering carbonate slope failure including sea level fall, seismic activity, storm or tsunami waves, and the development of overpressure (e.g. Bosellini, 1998; George et al., 1995; Spence and Tucker, 1997). Rusciadelli et al. (2003) used a two-dimensional finite difference approach to model the collapse of the Cretaceous Maiella platform margin. These authors explored the effects of loading due to sea level fall and seismic events, but did not explicitly incorporate effects of differential compaction into their model.

In this paper we use two-dimensional finite element modeling to explore the integrated effects of loading due to carbonate platform growth and steep slope angles on the synsedimentary deformation of carbonate platforms. The geometry and facies distribution of our model is based on the Capitan depositional system of West Texas and New Mexico, where the paucity of tectonic deformation, excellent outcrop exposure, and abundant previous work provide good constraints on platform to basin geometry and facies distribution. We use an elastic rheology in order to explore the distribution of stresses and displacements prior to failure. Model results suggest that steep-sloped carbonate reef complexes are inherently unstable and that differential displacements and stress concentrations, both differential and tensile, play an important role in the evolution of these systems. While we focus our attention on the Capitan system, conclusions drawn from examination of model results are relevant to the general case of steep-sloped carbonate margins.

## 2. Geologic background

The Permian Capitan depositional system has been the topic of numerous publications since the seminal work of King (1948). Here we briefly summarize the geologic elements pertinent to modeling and understanding synsedimentary deformation of the system: the regional structure, the dominant sedimentary facies and their present-day geometry, and synsedimentary deformational features. We refer interested readers to the brief review by Saller et al. (1999) that emphasizes ongoing controversies and the extensive review by Hill (1996) as well as the many works cited within these publications.

The Capitan system rims the Delaware Basin of West Texas and southeastern New Mexico, but only crops out in the Glass, Apache, and Guadalupe Mountains. The Guadalupe Mountains, extending over 70 km along strike with vertical relief locally exceeding a kilometer, provide the most extensive and spectacular outcrops of the Capitan depositional system (Fig. 1). Although the western end of the range is cut by numerous normal faults associated with Late Cenozoic Basin-and-Range extension, much of the remaining outcrop area shows little evidence of post-Permian deformation. A notable exception is the Huapache Monocline, a broad northeast dipping flexure located just east of Slaughter Canyon (Hayes, 1964).

The Capitan depositional system (Fig. 2) includes the Capitan reef/slope and the time-equivalent platform (Seven Rivers, Yates, and Tansill formations) and basin (Bell Canyon Formation) sediments (Saller et al., 1999). In the Guadalupe Mountains the Capitan reef aggraded ~300 m and prograded 4–5 km (Bebout et al., 1993; Tinker, 1998) over a basinward-thickening wedge of deep-water sediments (Garber et al., 1989) (Figs. 2 and 3). The Capitan reef and upper slope are interpreted as microbial boundstones with a bryozoan, sponge, and *Tubiphytes* framework (Kenter et al., 2005; Kirkland et al., 1998; Wood et al., 1996) that supported steep depositional slopes. The basinward face of the reef dips 40–80° (Kirkland et al., 1993, 1999) and upper slope deposits have dips that exceed 30–35° (Mruk and Bebout, 1993; Tinker, 1998). Equivalent lower-slope/basin sediments are dominated by carbonate wackestone and mudstone interbedded with basinal siltstones and channel-filling sandstones (Harms and Williamson, 1988). Age equivalent platform sediments include peloidal packstone and grainstone, ooid grainstone, and skeletal grainstone stacked in a series of cycle sets that are 10–20 m thick and laterally continuous across the platform (Osleger, 1998; Osleger and Tinker, 1999; Tinker, 1998). These carbonate cycle sets are typically bounded by meter-scale siliciclastic facies composed of fine-grained sandstone and siltstone. Platform cycle sets thicken and their dips progressively increase toward the platform edge, a geometry that has been termed "fall-in bed" by L.C. Pray (Hurley, 1978) (Fig. 3).

The platform and reef facies of the Capitan depositional system are cut by widespread reef parallel and reef perpendicular opening mode fractures (Hayes, 1964; Jagnow, 1979; King, 1948). Many of these fractures are filled with marine cements (Fig. 4A), skeletal carbonate sediments, and/or siliciclastic sediments (Fig. 4B) and are

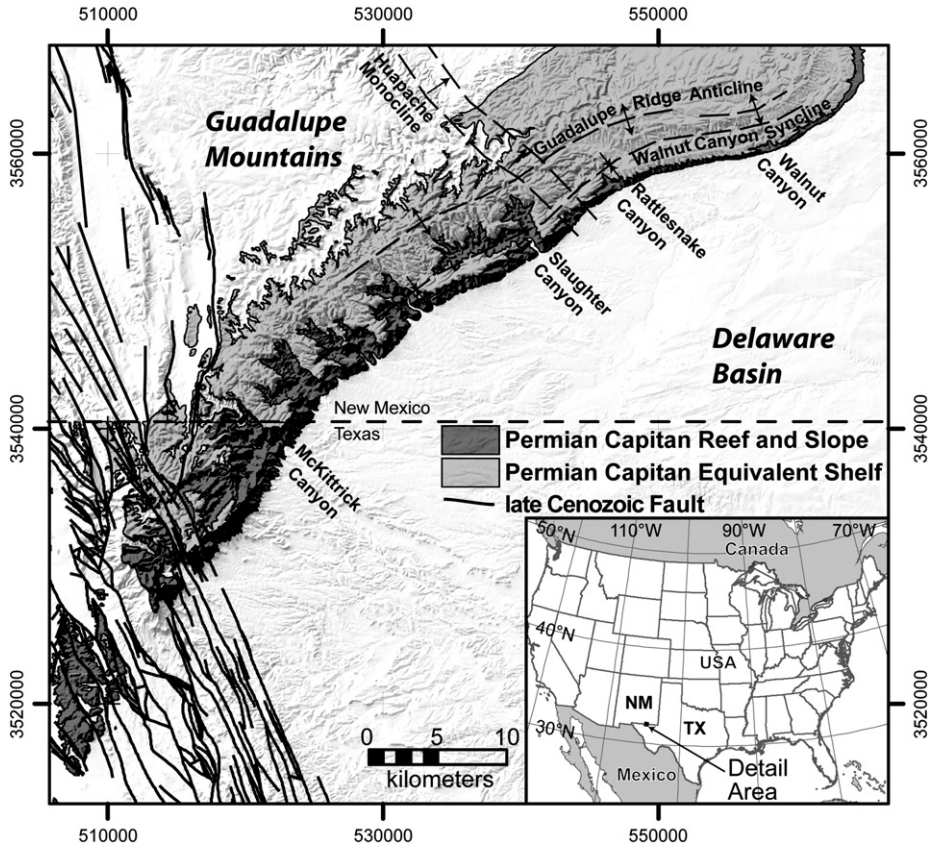


**Fig. 1.** Digital elevation model of the Guadalupe Mountains, west Texas and New Mexico. The northeast trending Permian Capitan reef margin prograded southeast toward the depths of the Delaware Basin. The present day configuration of the range is likely the result of Late Cenozoic Basin-and-Range tectonics, including north-northwest trending normal faults, the northwest trending Huapache monocline, and gentle northeast block tilting of the entire range. The two margin parallel folds, the Guadalupe Ridge anticline and Walnut Canyon syncline, likely resulted from differential compaction. Faults and bedrock geology for Texas after King (1948), and for New Mexico after Hayes (1964). Shaded relief derived from US Geological Survey 10 m digital elevation model. Map projection and coordinate system: Universal Transverse Mercator (UTM) zone 13, World Geodetic System 1984 datum, coordinates in meters.

thus demonstrably synsedimentary in origin (Stanton and Pray, 2004). These dikes are most common within ~100 m of the platform margin in the upper Yates and Tansill formations and are inferred to have formed in response to compaction of underlying sediments during rapid progradation and oversteepening of the platform margin (Stanton and Pray, 2004). The Capitan platform is also cut by a series of small to moderate offset faults (Fig. 4D and E), many of which are associated with growth strata (Hunt et al., 2002; Kosa and Hunt, 2005), growth folding (Fig. 3), and/or karst development and infilling of later platform sediments (Kosa and Hunt, 2006; Kosa et al., 2003) and were thus demonstrably active during deposition of Capitan-equivalent sediments. In lower-slope and basin facies, margin parallel fractures with wispy traces (Fig. 4C) and down-to-the-basin bedding plane slip surfaces (Brown and Loucks, 1993) are present.

A series of low-amplitude reef-margin parallel folds in the outer platform (Fig. 1) have been attributed to compaction-driven syn-sedimentary deformation (Hill, 1996). In the northeast Guadalupe

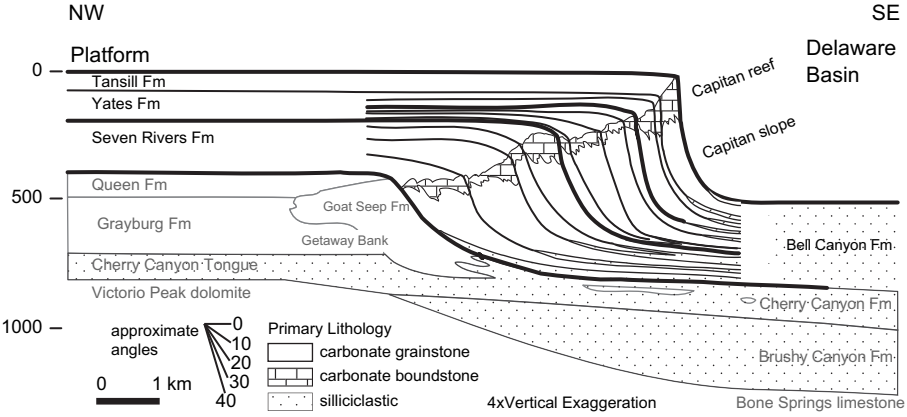


**Fig. 2.** Schematic cross-section highlighting stratal relations of the Permian Capitan system. The Capitan depositional system profile, in black, after Tinker (1998). Older Guadalupian sediments, in gray, after King (1948), Newell et al. (1953), Garber et al. (1989), Melim and Scholle (1999).

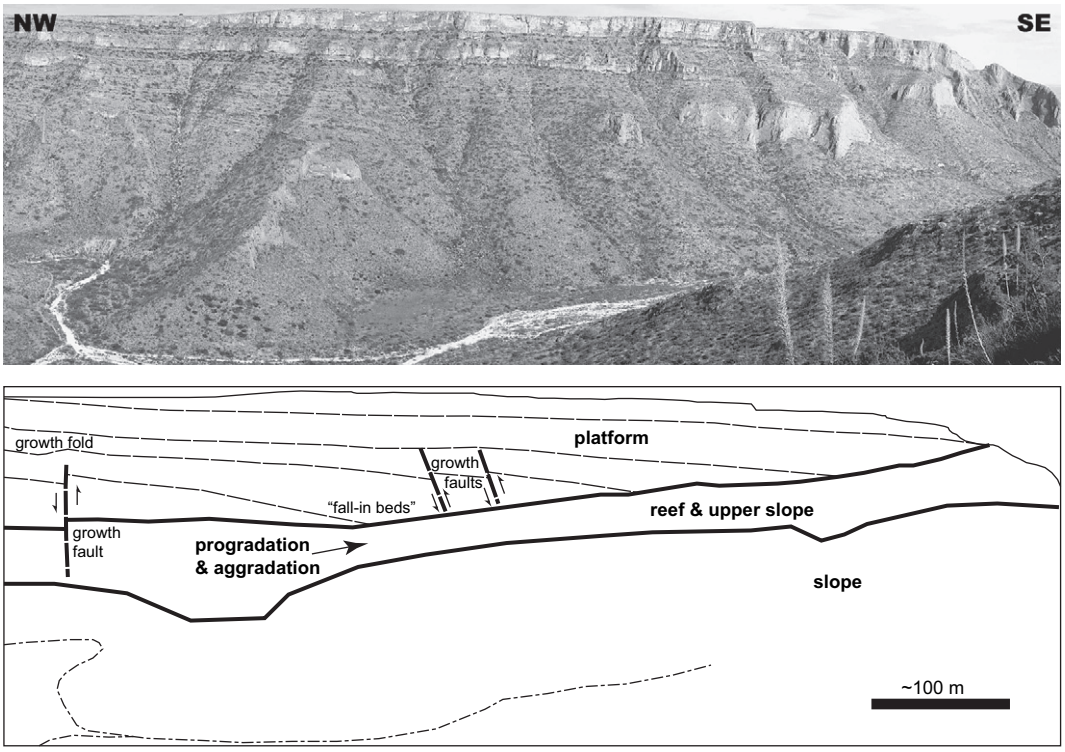


**Fig. 3.** Photo panorama of the northeast face of Slaughter Canyon. Line drawing at the bottom illustrates the progradational framework of the steep-sloped carbonate reef system. Note that distortions due to perspective make steep normal faults appear as thrust faults.

Mountains, the broad, northeast striking Guadalupe Ridge anticline is asymmetric in shape with a 1° northwest dip toward the platform and 6° southeast dip toward the basin. Southeast of this fold is the Walnut Canyon syncline, which shares the basinward dipping limb of the Guadalupe Ridge anticline and has a 1° northwest dipping southeast limb (Hayes, 1964). The development of fall-in bed geometry has also been cited as evidence of synsedimentary deformation (Hunt et al., 2002; Longley, 1999; Saller, 1996). However, a deformational origin remains controversial with many workers interpreting the basinward dips as primarily depositional in origin (e.g. Osleger, 1998; Tinker, 1998).

## 3. Geomechanical model

We have constructed a model of platform "growth" using the commercial finite element package, Abaqus®. We use linear elastic constitutive relations under two-dimensional plane–strain conditions. We construct the final model geometry in a step-wise manner, wherein each model layer is pre-stressed before "burial" by overlying strata, to mimic platform evolution. Previous workers (e.g. Chinnery, 1963; Pollard and Segall, 1987) have demonstrated the utility of elastic models for understanding incremental stresses and strains that appear critical in the accommodation and localization of permanent strains forming large-scale geologic structures. Elasticity is advantageous in that results are obtained with the input of three simple parameters only (two elastic constants and density), which are empirically well constrained. Coupled with variations in our model geometries, these three parameters yield many insights into deformation processes associated with these systems.

### 3.1. Model geometry and loading conditions

Our "base case" model is based on an idealized stratigraphic platform to basin cross-section from the Guadalupe Mountains to the Delaware Basin (Fig. 2). The model geometry consists of a preconditioning domain of variable margin geometry and an analysis domain of a fixed outer margin profile (Fig. 5). The preconditioning domain is required in order to minimize stress concentrations due to geometric complexities that would otherwise persist if the final configuration geometry were to be used from the beginning of the model run. It should be recognized that the initial preconditioning geometry influences the results in the analysis domain of the model. That is, a different initial (preconditioning) basal geometry would result in different final results. One might rationalize different initial geometries as being due to various scenarios of antecedent topography from which the reef system nucleates (e.g. Kerans and Tinker, 1999). In the case of the upper Permian Capitan system that is the focus of our modeling efforts, the step-wise evolution in our preconditioning domain (Fig. 5) attempts to capture the evolving steepening of lower-relief lower to middle Permian Victorio Peak and San Andres carbonate ramp systems to the higher-relief Goat Seep reef, all of which precede the growth of the Capitan system (Fig. 2). The analysis domain consists of an idealized platform to basin profile that is repeated with a 125 m horizontal and 12.5 m vertical offset to create a progradation to aggradation (P/A) ratio of 10 for the base case model. The vertical offset was chosen to approximate the 10–20 m cycle thickness of the Capitan platform.

The base of the model, below the preconditioning domain, is held fixed, whereas the sides of the model are laterally constrained, but free to move in the vertical direction. Loading is due solely to gravity and is applied as a body force to each element. The model is run in a step-wise manner, wherein successive layers are sequentially activated in the model and loaded (e.g. see step boundaries, Fig. 5). In practice, this is done by building a finite element mesh of the entire modeling domain and defining internal layering (both stratigraphic and step layering) within the full mesh geometry. Overall model dimensions are approximately 5 km in length and

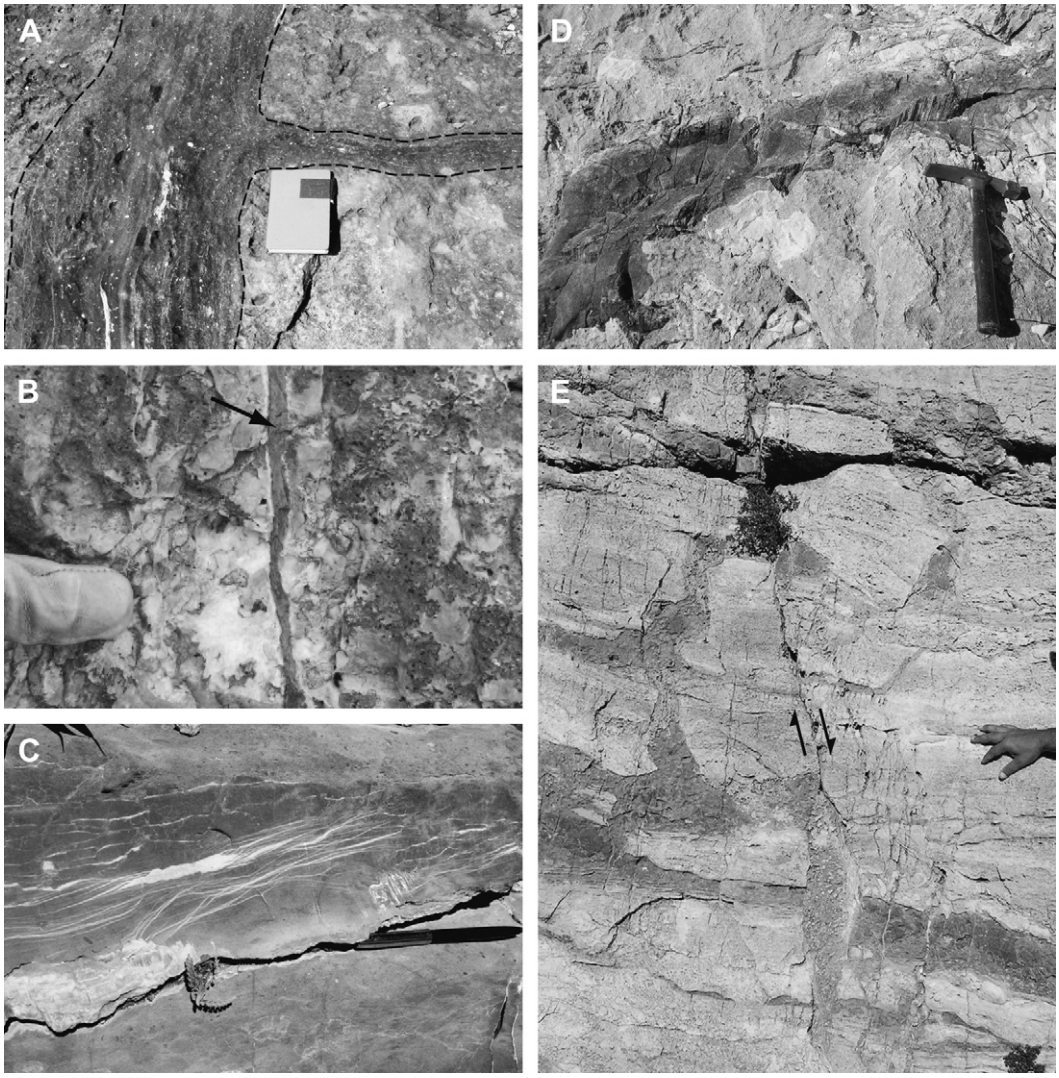


**Fig. 4.** Field examples of early-formed deformation features in the Permian Capitan reef complex. (A) Neptunian dike filled with early marine cement and *Archaeolithoporella* in Tansill-equivalent Capitan boundstone (reef), Bat Cave Draw outcrop near the mouth of Walnut Canyon. Photograph taken looking southwest. (B) Vertical fracture filled with platform-derived siliciclastics in Yates equivalent Capitan boundstone (reef), near the Permian Reef trail, McKittrick Canyon. Gloved finger for scale. Looking northeast. (C) Fracture clusters with wispy traces filled with calcite in Tansill-equivalent Lamar wackestone (slope), on the Permian Reef trail, McKittrick Canyon. Looking northwest. (D) Steeply dipping (~80°), reef-margin parallel syndepositional fault filled with siliciclastics in Yates platform sediments. Note slickenlines with steep rake above hammer. Near "Fault B" of Kosa and Hunt (2005), Slaughter Canyon. Looking north. (E) Steeply dipping, reef-margin parallel fault in Tansill platform sediments, Rattlesnake Canyon. Looking northeast.

range from 1 to 3 km in height, with an average element side-length of 3 m.

The step-wise implementation in Abaqus® leads to discontinuities in calculated displacement fields at the step boundaries. This effect is due to the fact that layers have zero displacement until activated, at which point they directly overlie layers with preexisting finite displacements. The continuous displacement field associated with addition of a new step is superimposed on the

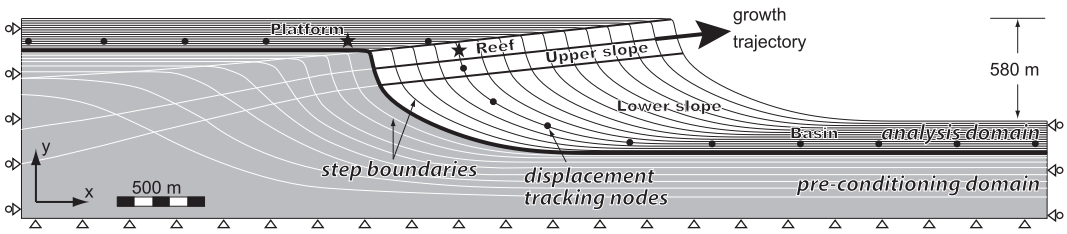


**Fig. 5.** Framework of model geometry used in finite element analysis showing major facies divisions. The illustrated geometry is for the strongly progradational base case model with a P/A = 10. The model is run step-wise in the direction of the growth trajectory. Note the distinction between the preconditioning domain (grayed area) and the analysis domain. Platform top to basin floor relief is 580 m. Heavy black dots are a portion of the node set used to track displacements along a step boundary. Black stars indicate the location of platform and reef stress tracking elements.

initial discontinuity, but the discontinuity remains throughout the model evolution.

It should be noted that a somewhat similar dog-toothed pattern is present in the calculated stress fields. However, this appears to be due to layer thickness, as defined by step size, and not due to the specific way that Abaqus® keeps track of the displacement values in the fixed mesh. In an effort to explore the effect of step size, we ran an alternate version of the base case scenario by adding two layers at a time. Results show that the dog-tooth pattern is accentuated with the larger step size and that stress magnitudes within each step layer are subdued. The corollary to this result is that an increasingly smaller step size would lead to smoother stress contours and more localized stress concentrations. We have chosen our base case step size for model efficiency and to mimic platform cycle-set thickness.

Four different geometric scenarios were constructed with varying progradation to aggradation ratios (Fig. 6). Systems with a low P/A ratio are primarily aggradational (e.g. Fig. 6A), while systems with a high P/A ratio are primarily progradational (e.g. Fig. 6D). In order to facilitate comparison of results between different model runs, an identical margin profile was used to construct each P/A scenario. Likewise, the step size in the direction of growth is the same for each model. However, for different P/A ratios, the same step size leads to relative differences in facies thicknesses. In the P/A = 10 case the reef facies is thickened with respect to the platform facies, while in the P/A = 0.1 case the opposite is true. This also leads to a different progradation style (Bosellini, 1984). The models with a low P/A ratio exhibit climbing progradation, while the models with a high P/A ratio exhibit horizontal progradation. The initial preconditioning step geometry was identical for each model and the remaining preconditioning steps facilitated a smooth transition from this base geometry into the constant P/A ratio for each model.

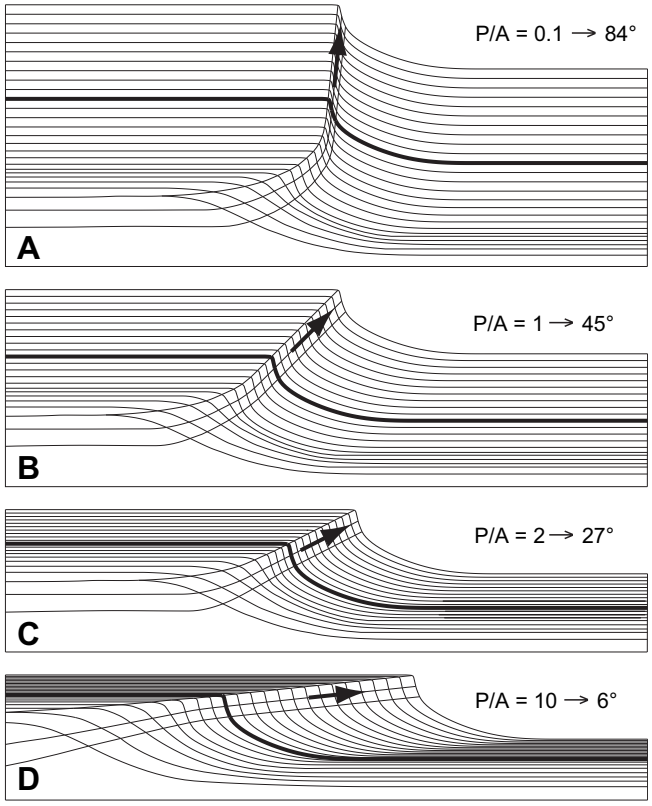


**Fig. 6.** Model geometries representing different progradation to aggradation (P/A) scenarios, from the (A) strongly aggradational system (P/A = 0.1) to the (D) strongly progradational (P/A = 10). Angles refer to the growth trajectory with respect to the horizontal.

### 3.2. Material properties

The model domain is subdivided into four regions based on sedimentary facies: platform, reef, upper slope, and lower-slope/basin. The dynamic elastic properties for each of these facies were calculated from ultrasonic velocity and rock density measurements of modern carbonate sediments using equations outlined in Mavko et al. (1998). Platform, reef and upper slope facies material properties are based on petrophysical studies by Anselmetti et al. (1997) and Incze (1998). These authors found that platform sediments are moderately compressible (Poisson's ratio of ~0.30) and are characterized by a wide range of Young's modulus, from ~5 GPa for loose sediments to >50 GPa for well-indurated samples. Dry rock densities vary with induration, ranging from 1700 to 2700 kg/m$^3$. On the other hand, reef and upper slope facies tend to be more uniformly stiff (Young's modulus of 20–50 GPa) and moderately compressible (Poisson's ratio of ~0.35) with dry rock densities of 2000–2700 kg/m$^3$. The lower-slope/basin facies incorporates fine-grained sediments deposited from distal debris flows and pelagic sedimentation. Material properties for this facies were adapted from studies of pelagic carbonate ooze in deep sea sediments by Milholland et al. (1980). According to their model, carbonate ooze buried to moderate depths (200–600 m) are relatively compliant (Young's modulus of ~1–4 GPa) and incompressible (Poisson's ratio of 0.40–0.465) with dry rock densities of 1600–1800 kg/m$^3$. The high incompressibility arises from the fact that these sediments are characterized by low permeability and high water saturation (Lavoie, 1988; Milholland et al., 1980). The material properties for the various facies used in our base case model are presented in Table 1.

Recognizing the fact that each facies is subject to a wide range of mechanical property values, we examined a number of scenarios by varying the values away from the base case in an effort to explore model sensitivities. For example, while we define the platform unit as a single facies with homogenous elastic parameters, we recognize that this facies in fact consists of a wide variety of lithofacies of varying abundance, from wackestone to packstone to grainstone, each with a distinctly different range of material property values.

## 4. Results

In the following section we present time stepped results for the base case model, highlighting the evolution of displacement patterns and stresses for a strongly prograding system. Plots of an exaggerated deformed profile (Fig. 7) for an early formed layer (see Fig. 5 for location) and color-contour plots of horizontal and vertical displacements (Fig. 8A and B) highlight evolving patterns of absolute and relative displacements. Stress results are presented

**Table 1**
Input parameters for the base case model.

| Facies | Dry density (kg/m$^3$) | Young's modulus (Pa) | Poisson's ratio | Source |
|---|---|---|---|---|
| Platform | 1600 | 1.0E+10 | 0.3 | A, I |
| Reef | 1900 | 3.5E+10 | 0.35 | A, I |
| Upper slope | 2100 | 4.5E+10 | 0.35 | I |
| lower slope and basin | 1800 | 4.0E+09 | 0.4 | M |

Key to source abbreviations: A, Anselmetti et al., 1997; I, Incze, 1998; M, Milholland et al., 1980.

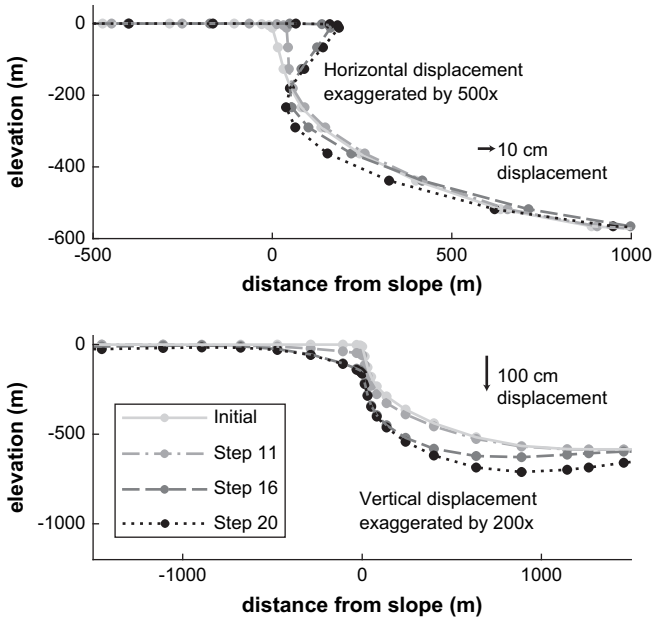


**Fig. 7.** Plots showing cumulative displacements in the P/A = 10 base case model scenario for three different time steps. The results are presented for the last run step using deformation superimposed on the P/A = 10 initial model geometry (see Fig. 5 for horizon location in the base case model) at the end of model time. Note that the displacements have been greatly exaggerated by variable factors to make the patterns of deformation visible. (A) Horizontal displacement. (B) Vertical displacement.

according to the engineering convention, where positive stress values indicate tension and negative values indicate compression. Color-contour plots of positive maximum Coulomb stress values, calculated from the complete stress tensor using a coefficient of friction of 0.85 (Byerlee, 1978), emphasize areas where faults are likely to initiate (Anderson, 1951). The Coulomb stress plots are overlain by a contour of 5 MPa in-plane tensile stress (Fig. 8C) to highlight areas of likely opening mode failure, based on typical tensile strength of carbonate rocks (Bell, 2000). This region of tensile failure is approximate, as tensile strengths of carbonate rocks may vary significantly from the mean value. We subsequently explore the sensitivity of these results to variations in material properties and changes in the P/A ratio presenting deformed profiles and stress plots for the final model solutions.

### 4.1. Base case

In the highly progradational base case model, the platform margin and reef are warped downward immediately after they are added to the model (Fig. 7, step 11) and continue to subside for ~5 steps as the reef progrades an additional ~600 m and aggrades ~60 m. Further model steps cause little additional differential subsidence of the platform margin. Maximum subsidence develops in the lower slope region after a period of burial (Figs. 7 and 8B). This area of subsidence widens with time starting at the middle slope and spreads basinward with further burial. Horizontal deformation (Figs. 7 and 8A) shifts the reef and outer platform toward the basin while displacing the lower slope in the opposite direction, toward the shelf. This deformation leads to a small clockwise rotation and additional steepening of the upper slope bedding. A region of basinward motion also develops below the lower slope after a period of burial.

Positive maximum Coulomb stresses (Fig. 8C) develop in the platform margin, upper slope, and in one small region of the reef face immediately after deposition. After additional burial, positive maximum Coulomb stresses develop in the reef and immediately adjacent platform and upper slope. These stresses increase in magnitude with further burial. In-plane tensile stresses exceeding 5 MPa (red contour, Fig. 8C) are also limited to the reef and develop only after a period of burial. Out-of-plane tensile stress develops in a pattern similar to in-plane tensile stress. However, the out-of-plane stresses are lower by a factor of four.

The orientation of in-plane principal stresses varies throughout the model domain (Fig. 9). Near the model surface, the maximum compressive stress is vertical within the platform facies. However, near the steep slope face within the reef and upper slope facies, the maximum compressive stress switches orientation to align parallel to the free surface. In the lower-slope/basin facies, the orientation of the maximum compressive stress remains parallel to the free surface for the outermost model layers, eventually leading to a horizontal maximum stress for the basin (Fig. 9). This stress pattern decays with depth so that at depths greater than approximately twice the platform to basin relief, the maximum compressive stress is vertical throughout the model. Slight changes in principal stress orientation also occur within and immediately below the reef and upper slope facies.

### 4.2. Effects of varying material properties

Material properties in the base case model were determined from the best available measurements of the elastic properties of carbonate sediments. These properties, however, often vary significantly within a given facies. Additionally, elastic properties of rocks are typically scale dependent with laboratory measurements of Young's modulus exceeding in situ measurements by up to two orders of magnitude (Pollard and Fletcher, 2005). We therefore developed a series of models to evaluate the effects of varying Poisson's ratio for the lower-slope/basin facies and Young's modulus for the lower-slope/basin facies and the platform facies.

The base case model uses a high value of Poisson's ratio (0.4) for the lower-slope/basin sediments. This value may be appropriate for undrained sediments. However, a more typical value for dry rock is 0.25. An even lower value (e.g. 0.1) may be appropriate for simulating compaction where sediments shorten in the direction of greatest compressive stress (typically vertical) without significant extension in other (i.e. lateral) directions. A series of models explores the effects of these lower values on displacements (Fig. 10A) and stresses (Fig. 11B and C). Reducing Poisson's ratio to 0.25 increases subsidence near the platform margin by ~60–70%. Reducing Poisson's ratio to 0.1 increases the subsidence in this region by an additional ~30%. In the case of high Poisson's ratio there is an apparent bulge (actually an area of lower subsidence) 700–1200 m shelfward of the platform edge. This effect is absent in models with lower Poisson's ratio and the overall zone of enhanced subsidence associated with the platform edge is thus wider by more than 1000 m. The region of basin floor subsidence at the toe-of-slope also increases in magnitude and broadens slightly with decreasing Poisson's ratio. Basinward displacement of the platform edge and upper slope is also enhanced by reducing the lower-slope/basin Poisson's ratio. Reducing Poisson's ratio in the basin extends the region of positive maximum Coulomb stress into the platform and broadens the region of tensile stress greater than 5 MPa (Fig. 11A, B, and C). In the case of extremely low Poisson's ratio, a new area of positive maximum Coulomb stress develops at the toe-of-slope (Fig. 11C).

Reducing Young's modulus in the lower-slope/basin facies creates a more compliant substrate for the carbonate platform and may therefore mimic the effects of sediment compaction. Reducing Young's modulus from 4 GPa (base case value) to 0.4 GPa increases subsidence at the platform margin by a factor of ~10 and at the

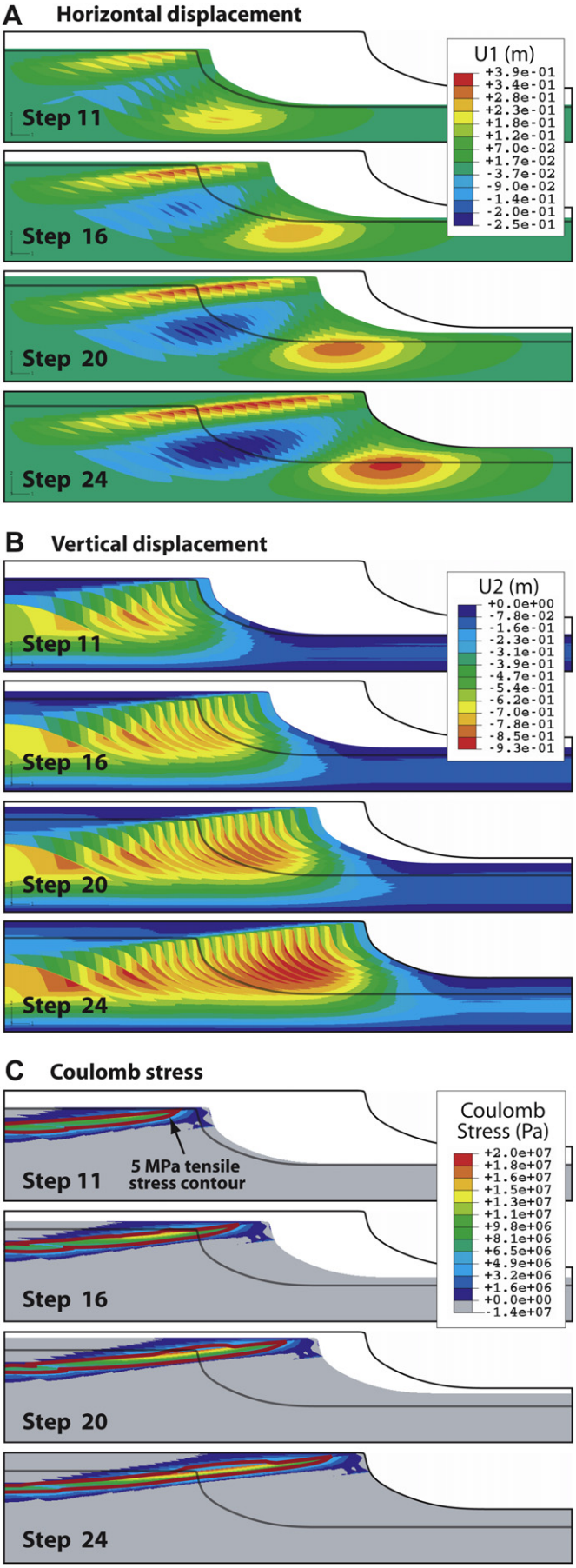


**Fig. 8.** Suite of results for four steps of the P/A = 10 base case model scenario. The gray line is the boundary between the model preconditioning domain and the analysis domain. (A) Maps of horizontal displacement (U1). Red colors indicate displacements towards the right, while blue colors indicate displacements towards the left. (B) Maps of vertical displacement (U2). (C) Maps of positive Coulomb stress. Red contour encloses region where in-plane tensile stress exceeds 5 MPa.

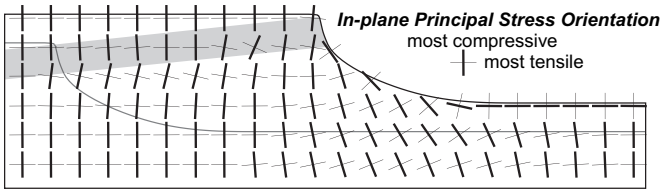


**Fig. 9.** Map of in-plane principal stress orientation for the P/A = 10 base case model scenario. Ticks lengths are set equal and do not reflect stress magnitude (see Fig. 8). The thin gray line is the boundary between the preconditioning and modeling domains. The gray-filled polygon is reef and upper slope facies. Principal stress orientations for the remainder of the model scenarios presented in this paper are qualitatively comparable to the P/A = 10 results.

toe-of-slope by a factor of ~8 (Fig. 10B). Further reducing Young's modulus to 0.04 GPa increases the subsidence by a factor of ~100 at the platform margin and ~80 at the toe-of-slope, a linear order of magnitude extrapolation from the 0.4 GPa case. The width of the zone of enhanced platform subsidence increases with reduced basin stiffness and appears to equal or exceed the model width for Young's modulus of 0.04 GPa. The width of the toe-of-slope region of subsidence appears to remain constant even though there is greater basin subsidence in the more compliant case. Reducing the lower-slope/basin stiffness also increases the basinward displacement of the platform margin and the shelfward displacement of the middle slope (Fig. 10B). A more compliant lower-slope/basin layer increases the magnitudes and expands the regions of positive maximum Coulomb stress and tensile stress greater than 5 MPa (Fig. 11A, D and E). For a lower-slope/basin Young's modulus of 0.04 MPa almost the entire platform would be expected to fail through shear and/or opening mode fracture.

While we define the platform unit as a single facies with homogenous elastic parameters, we recognize that this facies in fact consists of a wide variety of lithofacies of varying abundance, each with a distinctly different range of material properties. The base case model uses a relatively soft platform Young's modulus (10 GPa). A significantly softer platform, consistent with the softening effects of internal heterogeneities (e.g. sedimentary layering) increases platform subsidence by up to 200%, decreases platform margin subsidence by ~1% and increases toe-of-slope subsidence by ~1%. The softer platform increases the basinward motion of the platform margin by ~7% and decreases the shelfward displacement of the lower slope by ~3%. The softer platform reduces the regions of positive maximum Coulomb stress and tensile stress over 5 MPa in the platform (Fig. 11F). A stiffer platform with Young's modulus of 35 GPa, typical of carbonate hard grounds, reduces platform subsidence by ~20%, increases platform margin subsidence by ~2%, and decreases toe-of-slope subsidence by ~2%. Platform margin basinward horizontal displacements decrease by ~15%, while middle slope shelfward displacements increase by 10–15%. The stiffer platform generates a broader region of positive maximum Coulomb stress adjacent to the reef and a larger region of tensile stress over 5 MPa (Fig. 11G).

The choice of density value also affects the model results. Our base case model uses dry rock density to calculate body forces. Dry rock density values fall between saturated (dry rock density plus weight of pore fluids under saturated conditions) and buoyant

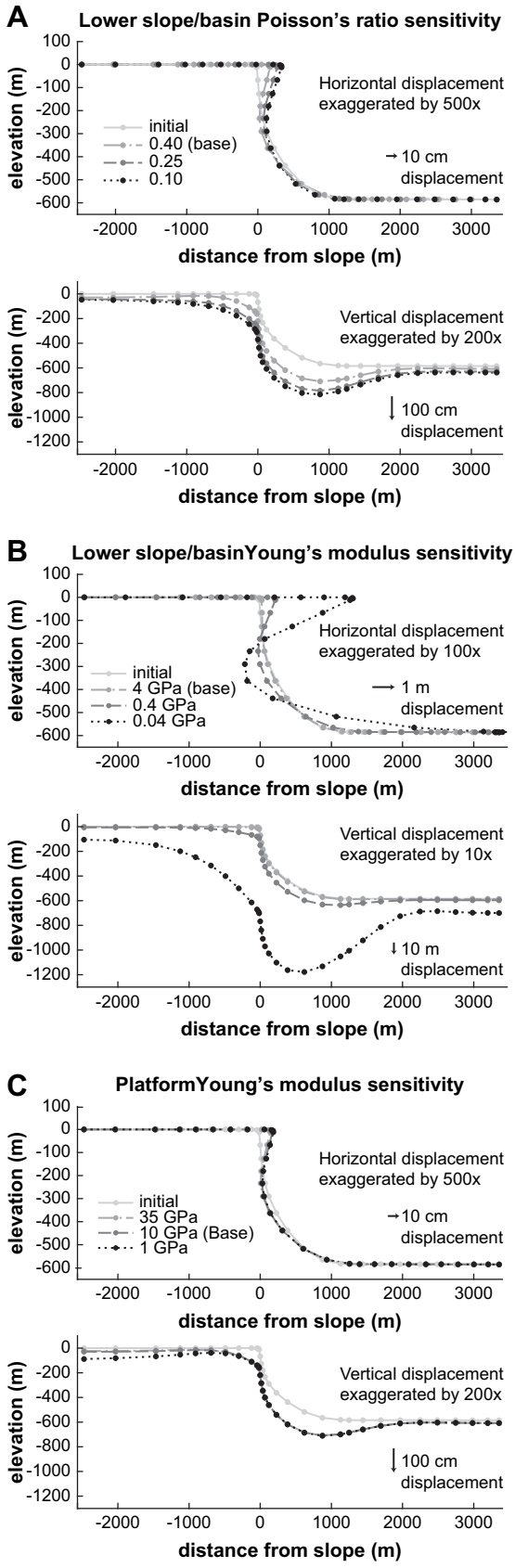


(saturated rock density minus water density) density values. The use of saturated density values for calculating body forces may be appropriate for conditions where fluids are trapped in the local pore space (undrained conditions) so that rock and fluid masses are linked. The use of saturated densities increases platform margin subsidence by ~45% and average least compressive stress values by ~20%. The use of buoyant density values may be appropriate for sediments sinking in a free-flowing fluid phase (drained conditions). The use of buoyant densities decreases platform margin subsidence by ~20% and average least compressive stress values by ~30%. Although the different density values affect the magnitudes of displacements and stresses the patterns remain largely unchanged.

### 4.3. Effects of varying progradation to aggradation ratio

The base case model has a P/A ratio of 10 which is on the order of the average P/A ratio of ~13 documented for the Capitan shelf margin in McKittrick Canyon (Tinker, 1998). P/A ratio within the Capitan depositional system, however, ranges from 3 to 37 for individual high-frequency sequences (Osleger, 1998; Osleger and Tinker, 1999; Tinker, 1998). Furthermore, other steep-sloped carbonate depositional systems are characterized by highly aggradational or even back-stepping intervals (e.g. Frost and Kerans, 2009; Kenter et al., 2005; Playford, 1984). We have constructed a series of four models with varying P/A ratio to explore the effects of this parameter on patterns of differential subsidence and stress. Although we have maintained a constant starting profile in the preconditioning steps and the same platform to basin profile in the analysis domain of the models, variations in thickness and model widths make direct quantitative comparison difficult. The following discussion therefore emphasizes patterns and relative magnitudes of displacement and stress rather than quantitative differences.

Absolute displacements in the models are controlled by the total sediment thickness which is a function of the P/A ratio in each model. In terms of relative displacement, however, all models develop a down-warp of the platform margin (Fig. 12) and slope. For low P/A models this area of subsidence is significantly wider than high P/A models. High P/A models thus develop pronounced downward tilting of the platform margin and the toe-of-slope region. All models also develop basinward motion of the platform edge. This effect is also more localized for the high P/A models. A horizontal displacement minimum occurs in the lower slope and a second basinward maximum is developed near the toe-of-slope for all models except for the P/A = 0.1 model. For this model, with the lowest P/A ratio, all horizontal motion is toward the basin. Displacements reach a maximum at the platform margin and then drop off quickly toward the basin.

Maximum Coulomb stress and tensile stress are lower in magnitude and less widely distributed in low P/A models in comparison to high P/A models (Fig. 13). The basic stress pattern for P/A = 2 is similar to that of the base case (P/A = 10) except that the stress magnitudes are greatly reduced and the region of tensile stress >5 MPa is reduced in area. For P/A = 1 the region of high tensile stress in the reef vanishes and high maximum Coulomb stresses are limited to the reef in the near surface and the near-reef platform. For P/A = 0.1, positive maximum Coulomb stresses are limited to the shallow platform, and the platform, reef, and slope near the (free) surface. Plots of stress evolution for individual tracking nodes (Fig. 14) show that platform and reef elements

**Fig. 10.** Plots of horizontal and vertical displacement illustrating model sensitivities for variations in rock mechanical properties. Refer to Fig. 7 for a detailed description of the plot. (A) Plots of models with different Poisson's ratio values in the lower-slope/basin facies. (B) Plots of models with different Young's modulus values in lower-slope/basin facies. (C) Plots of models with different Young's modulus values in the platform facies.

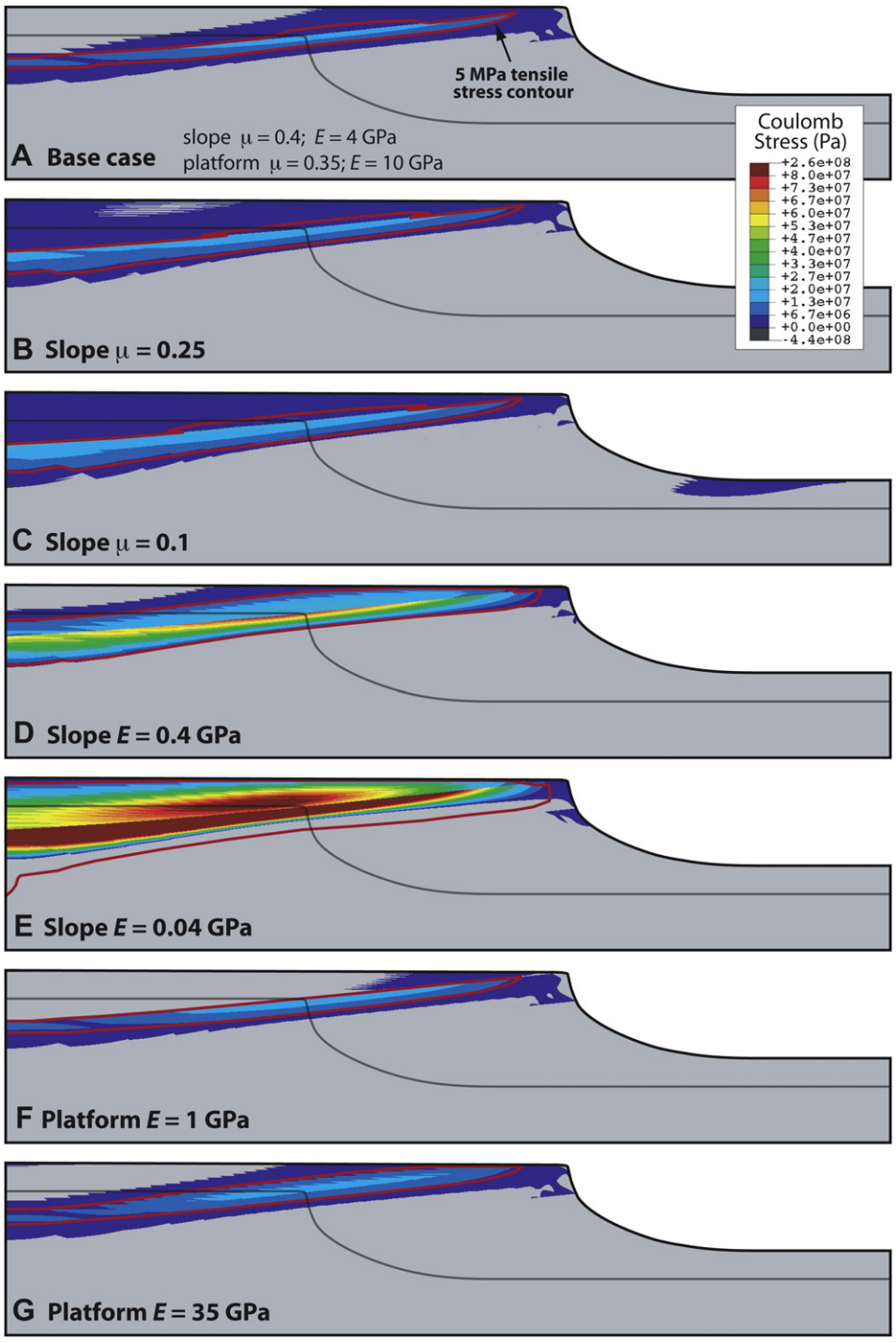


**Fig. 11.** Maps of Coulomb stress illustrating model sensitivities for variations in rock mechanical properties for the lower-slope/basin and platform facies. The red contour encloses the region where in-plane tensile stress exceeds 5 MPa. Only positive values of Coulomb stress are shown. Results are presented for the last run step using the P/A = 10 model geometry. The gray line is the boundary between the model preconditioning domain and the analysis domain. Refer to Table 1 for the rock mechanical properties used in the (A) base case model. Results for models with rock properties that depart from the base case model are shown in maps (B) to (G).

initially experience tensile (positive) stresses even in low P/A models. However, with burial, these stresses are reduced or become compressive (negative).

## 5. Discussion

The results of our step-wise model of carbonate platform development yield similar patterns of displacement and stress across orders of magnitude variations in material properties and progradation to aggradation ratio. Ubiquitous features of model results include: (1) a region of enhanced subsidence centered near the platform margin, (2) basinward displacement of the platform margin that decreases down slope, and (3) positive maximum Coulomb stress and positive (tensile) normal stress near the platform margin and in adjacent slope and platform facies. We interpret these results as further support for the contention of Hunt et al.

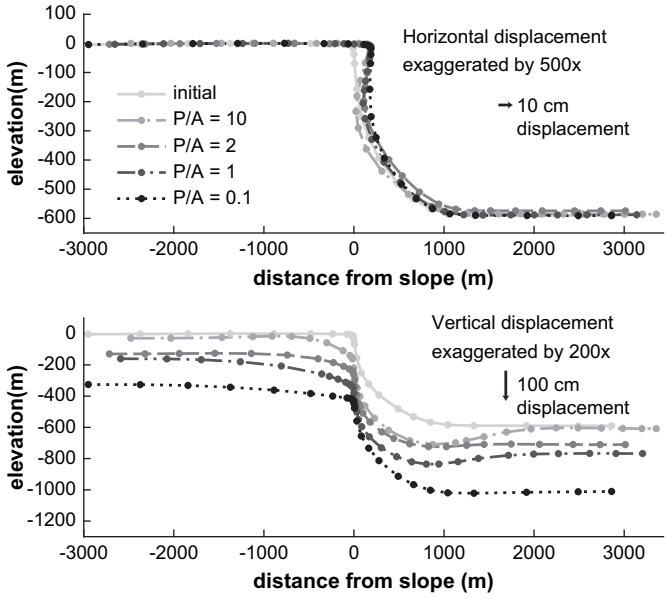


**Fig. 12.** Displacement plots for varying P/A ratios. Refer to Fig. 7 for a detailed description of the plot. Displacement tracking nodes in the P/A = 0.1, 1, and 2 models were chosen in a similar stratigraphic position to those in the P/A = 10 model. The absolute horizontal position of the individual model curves has been adjusted to keep the platform edge in the same position (both plots) and vertically (for vertical deformation) to clearly display the individual model geometries. See text for more detailed discussion.

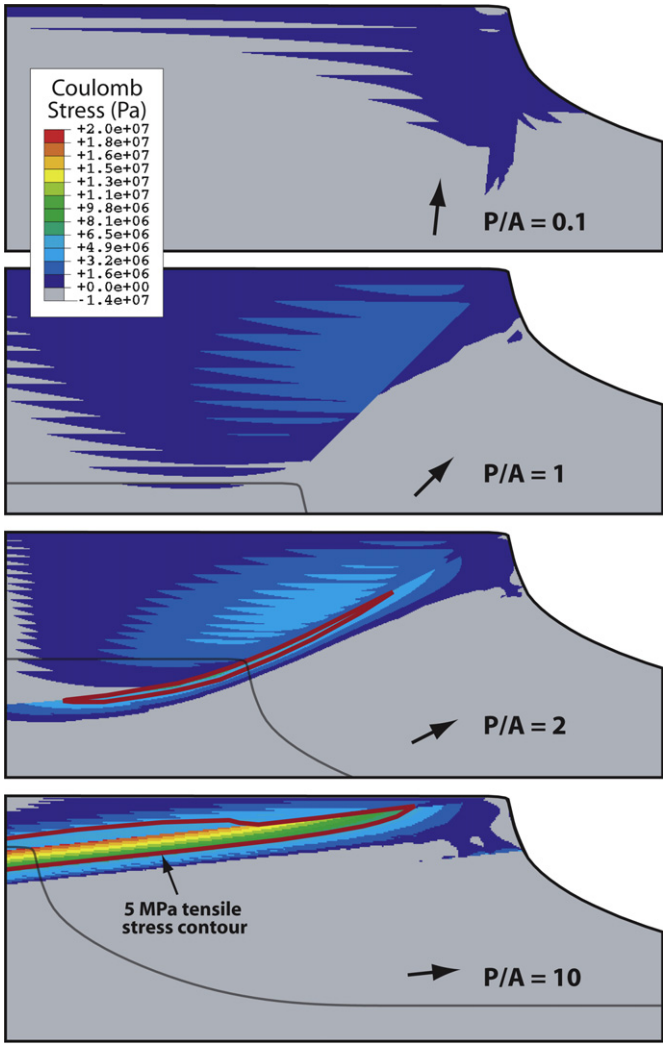


**Fig. 13.** Maps of Coulomb stress illustrating differences between model geometries with different P/A ratios. The red contour encloses the region where in-plane tensile stress exceeds 5 MPa. The results are presented for the last run step for each respective geometry. The gray line is the boundary between the model preconditioning domain and the analysis domain (not shown in the P/A = 0.1 case because it is outside the area of view). Only positive values of Coulomb stress are shown.

(1996) that compaction-related deformation can strongly influence the development of carbonate margins. The consistency of our model results suggest that synsedimentary deformation has likely modified all steep-sloped depositional geometries and is also likely to promote shear and opening mode failure near the platform margin.

In comparison with previous studies concerning the synsedimentary deformation of carbonate margins that have generally modeled compaction conceptually or through the use of one-dimensional porosity–depth relationships (Doglioni and Goldhammer, 1988; Longley, 1999; Marella et al., 2004; Rusciadelli and Di Simone, 2007; Saller, 1996; Tinker, 1998), our model treats carbonate strata as elastic materials that are able to transmit stresses vertically and laterally. Subsidence in our models, therefore, is not a direct function of the compressibility/compliance of sediments directly below a given location, but is dependent on the material properties and geometry of the strata within the entire system.

### 5.1. Impacts on stratal architecture

The patterns of deformation described above are strikingly similar to present-day stratal geometries of the Capitan depositional system. Specifically, our base case model predicts a small amount of inner platform subsidence, an outer platform high, down-warping of the platform margin, and steepening of upper slope bedding to form in response to gravity-driven deformation. Many of these features develop immediately upon "deposition" of a model layer and may therefore exist as basin floor features, however they are enhanced by additional burial during subsequent stages of platform growth.

The depositional geometry of the Capitan system, as well as the degree to which these geometries have been modified by post-depositional deformation, has been a long-standing topic of debate (see Saller et al. (1999) for a brief review). The depositional profile of the Capitan system has alternatively been interpreted as a continuous basinward slope (King, 1948), a barrier reef (Newell et al., 1953), or a marginal mound (Dunham, 1972). These models are partly based on sedimentary facies arguments, but also rely on interpretations of stratal geometry to infer paleo water depths (Hunt et al., 2002). Fine-grained cavity-filling sediments (geopetals) may provide an independent means for identifying the post-depositional rotation of carbonate sediments. Geopetal data from the Capitan depositional system have shown mixed results suggesting a largely depositional origin for fall-in beds in the Seven Rivers Formation (Hurley, 1978, 1989) and a largely deformational origin for tilting of Yates platform strata and Yates equivalent Capitan reef (Harwood and Kendall, 1999; Hunt et al., 2002; Saller, 1996). Although it is possible that Hurley's interpretation of geopetal data from the Seven Rivers Formation may be incorrect due to apparent dip effects (Hunt et al., 2002) our model results suggest that the relative contributions to outer platform geometry need not remain constant throughout the deposition of the Capitan system.

The consistency of our model results suggest that the use of present-day stratal geometries to infer original depositional

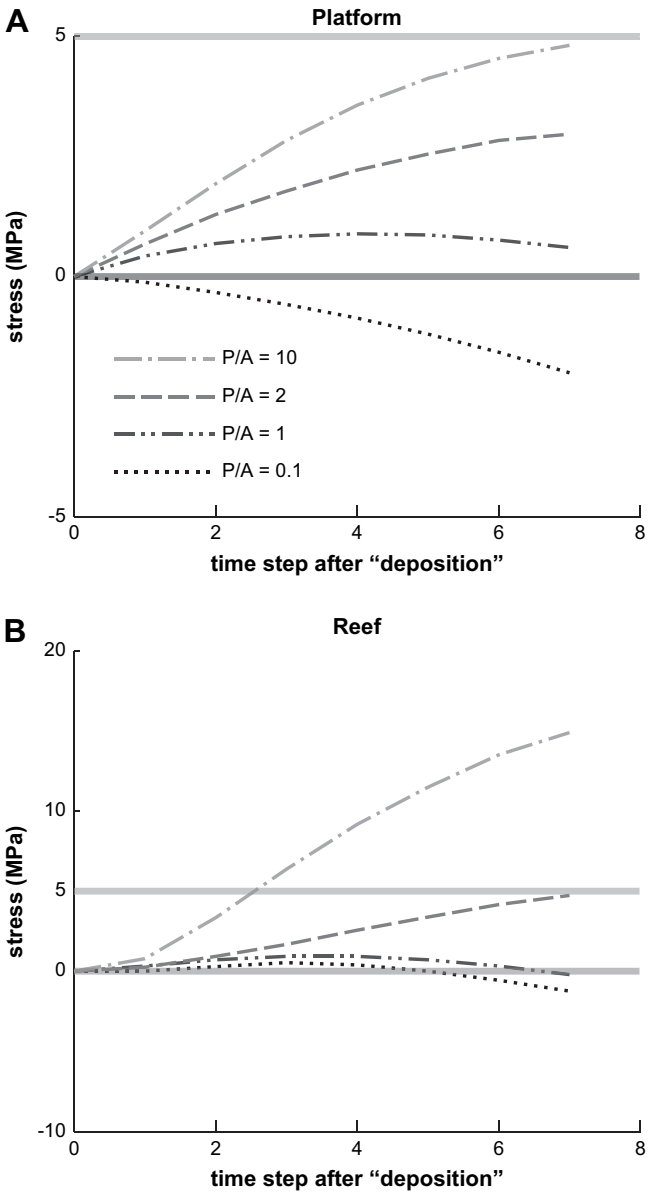


**Fig. 14.** Comparison of evolution of least compressive stress at select nodes for different P/A ratio scenarios. (A) Platform tracking node. (B) Reef tracking node. See Fig. 5 for the location of the nodes.

profiles should be approached cautiously. Platform stratal geometries likely form as the result of the interplay between patterns and rates of deformation and sedimentation. The elastic models presented in this study are useful for predicting patterns of incremental strain and stress, but are unable to capture time-dependent processes such as the flow of intergranular fluids (poroelasticity) or pressure solution (creep) that likely control the rates of compaction-driven subsidence. Incorporation of these time-dependent processes in future models may lead to a more complete understanding of the interplay between the processes that shape stratal geometry including rates of sedimentation, diagenesis, deformation, and sea level change.

### *5.2. Implications for synsedimentary deformation processes*

Although our models do not implicitly incorporate failure and accumulation of plastic strains, patterns of stress may be used to infer areas of likely failure and strain localization. Specifically, regions of high maximum Coulomb stress are likely to fail in shear, forming synsedimentary faults, whereas areas of tensile stress are likely to fail in opening mode, forming joints.

Regions of highest maximum Coulomb stress in our models are located at depth some distance behind the active reef front. The distance between the highest maximum Coulomb stress and the platform margin varies with changing P/A ratio. Field studies of the Capitan depositional system appear to corroborate this result. In Slaughter Canyon synsedimentary faults initiated 900–1400 m shelfward of Yates 2 reef, 800–900 m shelfward of Yates 4 reef, and 400–500 m shelfward of Tansill reef (Kosa and Hunt, 2005). Over this same depositional interval progradation was generally decreasing, although individual cycle sets, such as the Yates 4, had higher P/A ratios (Harris and Saller, 1999; Osleger, 1998; Osleger and Tinker, 1999; Tinker, 1998).

Nearly horizontal tensile stresses greater than 5 MPa, our assumed tensile strength for carbonates, develop in the reef and adjacent platform facies of our model after an incremental step of burial. Based on this result one might expect that near-vertical jointing occurs after burial and would not create open cracks at the sea floor. However, the occurrence of wide aperture joints (neptunian dikes) filled with platform and reef derived material (Devaney et al., 1986; Hunt et al., 2002; Playford, 1984; Stanton and Pray, 2004) demonstrate that open joints extended to the sea floor at the margins of several ancient steep-sloped carbonate systems. For joints in platform rocks, one might rationalize lower strengths that allow for failure to occur at reduced values of tensile stress (cf. Bell, 2000). On the other hand, strengths for reefal facies, where the majority of the neptunian dikes in the Capitan depositional system occur (Stanton and Pray, 2004), may exceed our assumed 5 MPa value due to early marine cementation. Possible explanations for this apparent discrepancy include the formation of joints in response to stress concentrations around abundant voids in reefal boundstones (e.g. Kirkland et al., 1993), propagation of joints upward in response to crack-tip stresses, development of additional tensile stress in association with slip along buried slope bedding planes (Playford, 1984), or in association with catastrophic failure of the steep reef front (Hine et al., 1992). Detailed field studies of fracture geometry and growth history may help determine which of these mechanisms are most important in the formation of neptunian dikes.

## 6. Conclusions

Using a step-wise elastic model of carbonate platform growth we have explored the integrated effects of compaction and slope geometry on the deformation of a steep-sloped carbonate system. Our models yield patterns of deformation similar to present-day stratal geometries of the Permian Capitan depositional system including platform margin subsidence or fall-in beds. We interpret these results as contributing to the growing body of evidence that gravity-driven synsedimentary deformation has likely modified all steep-sloped depositional geometries. Care should thus be taken when inferring paleo environmental characteristics from present-day stratal geometries. In addition, we interpret regions of positive maximum Coulomb stress and tensile stresses exceeding typical failure strength of carbonate rocks in our models as zones of likely brittle failure and suggest that these deformational features are also fundamental elements of steep-sloped carbonate platforms.

## Acknowledgements

This work benefited significantly from discussions with, and feedback from Wayne Narr. Thies Buchman assisted in the creation

of the initial step-wise geomechanical model geometry and the setup of the models in Abaqus®. Riccardo Caputo and David Osleger are thanked for providing thorough reviews. Acknowledgment is made to Chevron Energy Technology Company, the Donors of the American Chemical Society Petroleum Research Fund (to Resor), a Purdue Research Foundation Summer Faculty grant (to Flodin), and an Indiana University Intercampus Research Support Fund grant (to Flodin) for partial support of this research.

## References

Anderson, E.M., 1951. The Dynamics of Faulting and Dyke Formation, with Applications to Britain. Oliver and Boyd, Edinburgh.

Anderson, N.L., Franseen, E.K., 1991. Differential compaction of winnipegosis reefs - a seismic perspective. Geophysics 56 (1), 142–147.

Anselmetti, F.S., von Salis, G.A., Cunningham, K.J., Eberli, G.P., 1997. Acoustic properties of Neogene carbonates and siliciclastics from the subsurface of the Florida Keys: implications for seismic reflectivity. Marine Geology 144 (1-3), 9–31.

Audet, D.M., 1995. Modeling of porosity evolution and mechanical compaction of calcareous sediments. Sedimentology 42 (2), 355–373.

Bebout, D.G., Kerans, C., Harris, P.M., 1993. Introduction. In: Bebout, D.G., Kerans, C. (Eds.), Guide to the Permian Reef Geology Trail, McKittrick Canyon, Guadalupe Mountains National Park, West Texas. Guidebook 26. Bureau of Economic Geology, Austin, TX, pp. 1–4.

Bell, F.G., 2000. Engineering Properties of Soil and Rocks. Blackwell Publishers, Oxford, UK.

Bitzer, K., 1999. Two-dimensional simulation of clastic and carbonate sedimentation, consolidation, subsidence, fluid flow, heat flow and solute transport during the formation of sedimentary basins. Computers & Geosciences 25 (4), 431–447.

Bosellini, A., 1984. Progradation geometries of carbonate platforms – examples from the Triassic of the Dolomites, Northern Italy. Sedimentology 31 (1), 1–24.

Bosellini, A., 1998. Scalloped vs. faulted carbonate platform margins and the origin of basinal megabreccias. In: Bosellini, A., Stefani, M. (Eds.), Geology of the Dolomites, vol. 53. Memorie della Societa Geologica, Italiana, pp. 63–74.

Brown, A., Loucks, R.G., 1993. Toe of Slope. In: Bebout, D.G., Kerans, C. (Eds.), Guide to the Permian Reef Geology Trail, McKittrick Canyon, Guadalupe Mountains National Park, West Texas. Guidebook 26. Bureau of Economic Geology, Austin, TX, pp. 5–13.

Budd, D.A., 2001. Permeability loss with depth in the Cenozoic carbonate platform of west-central Florida. AAPG Bulletin 85 (7), 1253–1272.

Budd, D.A., 2002. The relative roles of compaction and early cementation in the destruction of permeability in carbonate grainstones: a case study from the Paleogene of west-central Florida, USA. Journal of Sedimentary Research 72 (1), 116–128.

Byerlee, J., 1978. Friction of rocks. Pure and Applied Geophysics 116 615–126.

Chinnery, M.A., 1963. The stress changes that accompany strike-slip faulting. Bulletin of the Seismological Society of America 53, 921–932.

Devaney, K.A., Wilkinson, B.H., van der Voo, R., 1986. Deposition and compaction of carbonate clinothems – the Silurian Pipe Creek Junior Complex of East-Central Indiana. Geological Society of America Bulletin 97 (11), 1367–1381.

Doglioni, C., Goldhammer, R.K., 1988. Compaction-induced subsidence in the margin of a carbonate platform. Basin Research 1 (4), 237–246.

Dugan, B., Flemings, P.B., 2000. Overpressure and fluid flow in the New Jersey continental, slope: implications for slope failure and cold seeps. Science 289 (5477), 288–291.

Dunham, R.J., 1972. Capitan Reef, New Mexico and Texas – facts and questions to aid interpretation and group discussion. Society of Economic Paleontologists and Mineralogists, Permian Basin Section, Publication, Midland. 72–14.

Frost, E.L., Kerans, C., 2009. Platform-margin trajectory as a control on syndepositional fracture patterns, Canning Basin, Western Australia. Journal of Sedimentary Research 79 (1–2), 44–55.

Fruth, L.S., Orme, G.R., Donath, F.A., 1966. Experimental compaction effects in carbonate sediments. Journal of Sedimentary Petrology 36 (3), 747–754.

Garber, R.A., Grover, G.A., Harris, P.M., 1989. Geology of the Capitan shelf margin; subsurface data from the northern Delaware Basin. In: Harris, P.M., Grover, G.A. (Eds.), SEPM Core Workshop, vol. 13, pp. 3–269.

George, A.D., Playford, P.E., Powell, C.M., 1995. Platform-margin collapse during Famennian reef evolution, Canning Basin, Western Australia. Geology 23 (8), 691–694.

Goldhammer, R.K., 1997. Compaction and decompaction algorithms for sedimentary carbonates. Journal of Sedimentary Research 67 (1), 26–35.

Grammer, G.M., Ginsburg, R.N., Swart, P.K., McNeill, D.F., Jull, A.J.T., Prezbindowski, D.R., 1993. Rapid growth rates of syndepositional marine aragonite cements in steep marginal slope deposits, Bahamas and Belize. Journal of Sedimentary Petrology 63 (5), 983–989.

Guidry, S.A., Grasmueck, M., Carpenter, D.G., Gombos, A.M., Bachtel, S.L., Viggiano, D.A., 2007. Karst and early fracture networks in carbonates, Turks and Caicos Islands, British West Indies. Journal of Sedimentary Research 77 (5–6), 508–524.

Halley, R.B., Schmoker, J.W., 1983. High-porosity cenozoic carbonate rocks of South Florida – progressive loss of porosity with depth. AAPG Bulletin 67 (2), 191–200.

Harms, J.C., Williamson, C.R., 1988. Deep-water density current deposits of Delaware Mountain Group (Permian), Delaware Basin, Texas and New Mexico. AAPG Bulletin 72 (3), 299–317.

Harris, P.M., Saller, A.H., 1999. Subsurface expression of the Capitan depositional system and implications for hydrocarbon reservoirs, northeastern Delaware Basin. In: Saller, A.H., Harris, P.M., Kirkland, B.L., Mazzullo, S.J. (Eds.), Geologic Framework of the Capitan Reef. SEPM Special Publication No. 65, pp. 37–49.

Harwood, G.M., Kendall, A.C., 1999. Reef margin collapse, gully formation and filling within the Permian Capitan reef: Carlsbad Caverns, New Mexico, USA. Sedimentology 46, 443–461.

Hayes, P.T., 1964. Geology of the Guadalupe Mountains, New Mexico, Professional Paper 446. US Geological Survey.

Heydari, E., 2000. Porosity loss, fluid flow, and mass transfer in limestone reservoirs: application to the Upper Jurassic Smackover Formation, Mississippi. AAPG Bulletin 84 (1), 100–118.

Hill, C.A., 1996. Geology of the Delaware Basin Guadalupe, Apache, and Glass Mountains New Mexico and West Texas. Society of Economic Paleontologists and Mineralogists. Permian Basin Section, Midland.

Hine, A.C., Locker, S.D., Tedesco, L.P., Mullins, H.T., Hallock, P., Belknap, D.F., Gonzales, J.L., Neumann, A.C., Snyder, S.W., 1992. Megabreccia shedding from modern, low-relief carbonate platforms, Nicaraguan Rise. Geological Society of America Bulletin 104 (8), 928–943.

Hunt, D., Fitchen, W.M., 1999. Compaction and the dynamics of carbonate-platform development; insights from the Permian Delaware and Midland basins; southeastern New Mexico and West Texas, U.S.A. In: Harris, P.M., Saller, A.H., Simo, J.A. (Eds.), Advances in Carbonate Sequence Stratigraphy; Application to Reservoirs, Outcrops and Models. SEPM Special Publication No. 63, pp. 75–106.

Hunt, D., Allsop, T., Swarbrick, R.E., 1996. Compaction as a primary control on the architecture and development of depositional sequences; conceptual framework, applications and implications. In: Howell, J.A., Aitken, J.F. (Eds.), High Resolution Sequence Stratigraphy; Innovations and Applications. Geological Society Special Publications, No. 104, pp. 321–345.

Hunt, D.W., Fitchen, W.M., Kosa, E., 2002. Syndepositional deformation of the Permian Capitan reef carbonate platform, Guadalupe Mountains, New Mexico, USA. Sedimentary Geology 154 (3-4), 89–126.

Hurley, N.F., 1978. Facies mosaic of the lower Seven Rivers Formation (Permian), North McKittrick Canyon, Guadalupe Mountains, New Mexico. Unpublished MS thesis, University of Wisconsin at Madison, WI.

Hurley, N.F., 1989. Facies mosaic of the lower Seven Rivers Formation, McKittrick Canyon, New Mexico. In: Harris, P.M., Grover, G.A. (Eds.), Subsurface and Outcrop Examination of the Capitan Shelf Margin, Northern Delaware Basin 13. SEPM Core Workshop, pp. 325–346.

Incze, M.L., 1998. Petrophysical properties of shallow-water carbonates in modern depositional and shallow subsurface environments. Unpublished PhD thesis, University of Miami, FL.

Jagnow, D.H., 1979. Cavern Development in the Guadalupe Mountains. Cave Research Foundation, Columbus, OH.

Kenter, J.A.M., 1990. Carbonate platform flanks – slope angle and sediment fabric. Sedimentology 37 (5), 777–794.

Kenter, J.A.M., Harris, P.M., Della Porta, G., 2005. Steep microbial boundstone-dominated platform margins – examples and implications. Sedimentary Geology 178 (1–2), 5–30.

Kerans, C., Tinker, S.W., 1999. Extrinsic stratigraphic controls on development of the Capitan reef complex. In: Saller, A.H., Harris, P.M., Kirkland, B.L., Mazzullo, S.J. (Eds.), Geologic Framework of the Capitan Reef. SEPM Special Publication No. 65, pp. 37–49.

King, P.B., 1948. Geology of the Southern Guadalupe Mountains, Texas. US Geological Survey Professional Paper P-215, 183 pp.

Kirkland, B.L., Longacre, S.A., Stoudt, E.L., 1993. Reef. In: Bebout, D.G., Kerans, C. (Eds.), Guide to the Permian Reef Geology Trail, McKittrick Canyon, Guadalupe Mountains National Park, West Texas. Guidebook 26. Bureau of Economic Geology, Austin, TX, pp. 23–30.

Kirkland, B.L., Dickson, J.A.D., Wood, R.A., Land, L.S., 1998. Microbialite and microstratigraphy: the origin of encrustations in the middle and upper Capitan Formation, Guadalupe Mountains, Texas and New Mexico, USA. Journal of Sedimentary Research 68 (5), 956–969.

Kirkland, B.L., Longacre, S.A., Stoudt, E.L., 1999. The dynamic Capitan Reef; an image of an ancient reef and suggestions for future research. In: Saller, A.H., Harris, P.M., Kirkland, B.L., Mazzullo, S.J. (Eds.), Geologic Framework of the Capitan Reef. SEPM Special Publication No. 65, pp. 161–173.

Kosa, E., Hunt, D.W., 2005. Growth of syndepositional faults in carbonate strata: Upper Permian Capitan platform, New Mexico, USA. Journal of Structural Geology 27 (6), 1069–1094.

Kosa, E., Hunt, D.W., 2006. Heterogeneity in fill and properties of Karst-modified syndepositional faults and fractures: Upper Permian Capitan Platform, New Mexico, USA. Journal Of Sedimentary Research 76 (1–2), 131–151.

Kosa, E., Hunt, D.W., Fitchen, W.M., Bockel-Rebelle, M.O., Roberts, G., 2003. The heterogeneity of Paleocavern systems developed along Syndepositional Faults; Upper Permian Capitan platform, New Mexico, USA. In: Ahr, W.M., Harris, P.M., Morgan, W.A., Sommerville, I.D. (Eds.), Permo-Carboniferous Carbonate Platforms and Reefs, Special Publication 78, Memoir 83. Society of Economic Paleontologists and Mineralogists & the American Association of Petroleum Geologists, pp. 291–322.

Lavoie, D., 1988. Geotechnical properties of sediments in a carbonate-slope environment: ODP Site 630, Northern Little Bahama Bank, in: Austin, J.A., Schllager,

W. (Eds.), Proceedings of the Ocean Drilling Program Scientific Results 101, pp. 315–326.
Longley, A.J., 1999. Differential compaction and its effects on the outer shelf of the Permian Capitan reef complex, Guadalupe Mountains, New Mexico. In: Saller, A.H., Harris, P.M., Kirkland, B.L., Mazzullo, S.J. (Eds.), Geologic Framework of the Capitan Reef. SEPM Special Publication No. 65, pp. 85–105.
Marella, C., Caputo, R., Bosellini, A., 2004. Growth and subsidence of carbonate platforms; numerical modelling and application to the Dolomites, Italy. Annals of Geophysics 47 (5), 1581–1595.
Mavko, G., Mukerji, T., Dvorkin, J., 1998. The Rock Physics Handbook; Tools for Seismic Analysis in Porous Media. Cambridge University Press, Cambridge, UK.
Melim, L.A., Scholle, P.A., 1999. Diagenesis of the Capitan Formation forereef facies (Permian, west Texas and New Mexico). In: Saller, A.H., Harris, P.M., Kirkland, B.L., Mazzullo, S.J. (Eds.), Geologic Framework of the Capitan Reef. SEPM Special Publication No. 65, pp. 193–210.
Milholland, P., Manghnani, M.H., Schlanger, S.O., Sutton, G.H., 1980. Geoacoustic modeling of deep-sea carbonate sediments. Journal of the Acoustical Society of America 68 (5), 1351–1360.
Mruk, D., Bebout, D.G., 1993. Slope. In: Bebout, D.G., Kerans, C. (Eds.), Guide to the Permian Reef Geology Trail, McKittrick Canyon, Guadalupe Mountains National Park, West Texas. Guidebook 26. Bureau of Economic Geology, Austin, TX, pp. 14–22.
Newell, N.D., Bradley, J.S., Whiteman, A.J., Fischer, A.G., 1953. The Permian Reef Complex of the Guadalupe Mountains Region, Texas and New Mexico; a Study in Paleoecology. W.H. Freeman & Co, San Francisco, CA.
Osleger, D.A., 1998. Sequence architecture and sea-level dynamics of Upper Permian shelfal facies, Guadalupe Mountains, Southern New Mexico. Journal of Sedimentary Research 68 (2), 327–346.
Osleger, D.A., Tinker, S.W., 1999. Three-dimensional architecture of upper Permian high-frequency sequences, Yates-Capitan shelf margin, Permian Basin, USA. In: Harris, P.M., Saller, A.H., Simo, J.A. (Eds.), Advances in Carbonate Sequence Stratigraphy: Application to Reservoirs, Outcrops, and Models. SEPM Special Publication No. 33, pp. 169–185.
Playford, P.E., 1984. Platform margins, Devonian reef complexes, in: Purcell, P.G. (Ed.), The Canning Basin, W.A. Proceedings of Geological Society of Australia/ Petroleum Exploration Society of Australia Limited, Perth, pp. 189–214.
Pollard, D.D., Fletcher, R.C., 2005. Fundamentals of Structural Geology. Cambridge University Press, Cambridge, UK.
Pollard, D.D., Segall, P., 1987. Theoretical displacements and stresses near fractures in rock: with applications to faults, joints, veins, dikes, and solution surfaces. In: Atkinson, B.K. (Ed.), Fracture Mechanics of Rock. Academic Press Inc., London, pp. 277–349.
Rusciadelli, G., Di Simone, S., 2007. Differential compaction as a control on depositional architectures across the Maiella carbonate platform margin (central Apennines, Italy). Sedimentary Geology 196 (1–4), 133–155.
Rusciadelli, G., Sciarra, N., Mangifesta, M., 2003. 2D modelling of large-scale platform margin collapses along an ancient carbonate platform edge (Maiella Mt., Central Apennines, Italy): geological model and conceptual framework. Palaeogeography Palaeoclimatology Palaeoecology 200 (1–4), 245–262.
Saller, A.H., 1996. Differential compaction and basinward tilting of the prograding Capitan reef complex, Permian, West Texas and Southeast New Mexico, USA. Sedimentary Geology 101 (1–2), 21–30.
Saller, A.H., Harris, P.M., Kirkland, B.L., Mazzullo, S.J., 1999. Geological framework of the Capitan depositional system – previous studies, controversies, and contents of this Special Publication. In: Saller, A.H., Harris, P.M., Kirkland, B.L., Mazzullo, S.J. (Eds.), Geologic Framework of the Capitan Reef. SEPM Special Publication No. 65, pp. 1–13.
Schlager, W., Camber, O., 1986. Submarine slope angles, drowning unconformities, and self-erosion of limestone escarpments. Geology 14 (9), 762–765.
Shinn, E.A., Robbin, D.M., 1983. Mechanical and chemical compaction in fine-grained shallow-water limestones. Journal of Sedimentary Petrology 53 (2), 595–618.
Shinn, E.A., Halley, R.B., Hudson, J.H., Lidz, B.H., 1977. Limestone compaction – enigma. Geology 5 (1), 21–24.
Spence, G.H., Tucker, M.E., 1997. Genesis of limestone megabreccias and their significance in carbonate sequence stratigraphic models: a review. Sedimentary Geology 112 (3–4), 163–193.
Stanton, R.J., Pray, L.C., 2004. Skeletal-carbonate neptunian dikes of the Capitan Reef: Permian, Guadalupe Mountains, Texas, U.S.A. Journal of Sedimentary Research 74 (6), 805–816.
Tinker, S.W., 1998. Shelf-to basin facies distributions and sequence stratigraphy of a steep-rimmed carbonate margin: capitan depositional system, McKittrick Canyon, New Mexico and Texas. Journal of Sedimentary Research 68 (6), 1146–1174.
Wood, R., Dickson, J.A.D., Kirkland, B.L., 1996. New observations on the ecology of the Permian Capitan reef, Texas and New Mexico. Palaeontology 39, 733–762.